



Article

Southern South American Long-Distance Pollen Dispersal and Its Relationship with Atmospheric Circulation

Claudio F. Pérez ^{1,2,*} , Ana G. Ulke ¹ and María I. Gassmann ^{1,2}

¹ Departamento de Ciencias de la Atmósfera y los Océanos, Facultad de Ciencias Exactas y Naturales, Universidad de Buenos Aires, Intendente Güiraldes 2160, Ciudad Universitaria, C1428 EHA, CABA, Argentina

² Consejo Nacional de Investigaciones Científicas y Técnicas, Godoy Cruz 2290, C1425 FQB, CABA, Argentina

* Correspondence: perez@at.fcen.uba.ar; Tel.: +54-9-11-41703839

Abstract: This paper addresses the study of synoptic-scale meteorological conditions that favor long-range pollen transport in southern South America combining airborne pollen counts, modeled three-dimensional backward trajectories, and synoptic and surface meteorological data. *Alnus* pollen transport trajectories indicate origins predominantly in montane forests of the Yungas between 1500 and 2800 m altitude. The South American Low-Level Jet is the main meteorological feature that explains 64% of the detected pollen arrival at the target site. *Podocarpus* and *Nothofagus* pollen instead are linked primarily to the widespread Subantarctic forests in southern Patagonia. Their transport patterns are consistent with previous studies, which show an association with synoptic patterns related to cold front passages carrying pollen in the free atmosphere (27% for *Nothofagus* and 25% for *Podocarpus*). These results show the significance of understanding long-distance pollen transport for disciplines such as climate change reconstruction and agriculture, emphasizing the need for further research to refine atmospheric circulation models and refine interpretations of past vegetation and climate dynamics.

Keywords: airborne pollen tracers; atmospheric circulation; SAMS; South America; *Alnus acuminata*; *Nothofagus*



Citation: Pérez, C.F.; Ulke, A.G.; Gassmann, M.I. Southern South American Long-Distance Pollen Dispersal and Its Relationship with Atmospheric Circulation. *Aerobiology* **2024**, *2*, 85–104. <https://doi.org/10.3390/aerobiology2040007>

Academic Editor: Olga Sozinova

Received: 28 July 2024

Revised: 3 September 2024

Accepted: 12 September 2024

Published: 12 October 2024



Copyright: © 2024 by the authors. Licensee MDPI, Basel, Switzerland. This article is an open access article distributed under the terms and conditions of the Creative Commons Attribution (CC BY) license (<https://creativecommons.org/licenses/by/4.0/>).

1. Introduction

Atmospheric pollen transport is of great interest in many aspects, from the purely academic, as in the case of the theory of pollen analysis that supports palaeoenvironmental reconstructions [1–7], to social ones like the treatment of respiratory allergies [8–13]. In these studies, there has been a demand for modeling, leading to the analysis of the relationships between meteorological variables, such as precipitation, temperature, and pollen emission. When models are applied, researchers must consider local pollen emissions and more complex processes involving wind-driven material from distant sources. Generally, distant sources have a low pollen contribution to the pollen sum of a given site and can be neglected without major consequences, but there are exceptional events of remarkable impact, as reported by some authors [14–16].

Investigating long-distance pollen transport is much more difficult in low latitudes because, although it is more diverse, the flora from tropical or subtropical regions is not commonly wind-pollinated. Conversely, at mid or high latitudes, this pollination syndrome is very extended, the vegetation includes fewer species, occupies wide regions, and long-range transport is easily observed. As a component of atmospheric aerosols, airborne pollen is considered the largest biological particle of the size spectrum [17] that could be used as a proxy of atmospheric circulation [18]. Usually, the preferred study technique comprises meteorological models employed in air pollution or environmental issues, within which Gaussian, Eulerian, or Lagrangian approaches are the most widely used. A comprehensive

list of model categories can be found in Fraile et al. (2006) [18] and the feasibility of simulating pollen transport was also thoroughly evaluated by Sofiev et al. (2006) [19].

Many case studies document long-range pollen transport in the Northern Hemisphere, for example, those reporting pollen arrivals to the high Arctic, Greenland, or the North Pole [20–22], or into the Mediterranean [23–26] among many others. On the contrary, there are few studies on this topic in South America. It is important to mention those who analyze the source–receptor relationship of pollen from extra-regional origin [27], the atmospheric mechanisms involved in trans-Andean pollen transport [28], and the role of transient weather systems defining the pollen source area in northern Patagonia [29]. Only one study accounts for bioaerosol dispersal concerning subtropical atmospheric circulation. Meza Torres et al. (2015) [30] first analyzed the combined effect of trade winds and the South American Monsoon as a possible dispersal pathway of *Ophioglossum reticulatum* L. fern spores coming from Northwestern Africa.

This paper addresses studying the main circulation patterns and synoptic-scale meteorological conditions that favor long-range pollen transport in southern South America. To complete this task, we carried out an interdisciplinary study with aerobiological sampling techniques using airborne pollen as atmospheric circulation tracers and numerical modeling of trajectories commonly used in meteorology.

2. Main Features of Atmospheric Circulation in Southern South America

Regional variations in South America's weather are the direct consequence of the land–ocean distribution, the mean climatic conditions, and the regular cycles at different timescales in the Southern Hemisphere. Diverse patterns from tropical to midlatitude zones arise from the latitudinal span of the continent (12° N–56° S). The Andes constitute a barrier to the zonal tropospheric flow producing dry conditions on the western slope and moist on the eastern slope in the subtropics [31]. A reversed pattern appears south of 35° S. Andean ranges also lead to intense tropical–extratropical interactions to the east, which characterizes the weather and climate of the Pampa plain and Patagonia plateau. Midlatitude synoptic variability shows different pressure patterns from which the main one represents the characteristic westerly flow south of 40° S [32]. The second variability mode represents equatorward cold-air outbreaks occurring all year round at 1- or 2-week intervals [32]. Its seasonal structure has modest changes although the interaction with warm and humid subtropical air masses in summertime leads to stronger convective processes [33,34]. Cold fronts also deeply impact the surface temperature mainly in wintertime when extremely persistent episodes produce intense freezing conditions in central-southern South America [35,36].

North of 35° S and east of the Andes, the most significant feature of the atmospheric circulation is the seasonal moisture, heat, and pressure, horizontal and vertical changes involved in the South American Monsoon System (SAMS) [37]. The South American Low-Level Jet (SALLJ) is a component of the SAMS that has been extensively studied due to its role in the hydrological cycle of Southeastern South America (SESA) [38]. Specifically, the SALLJ is the strengthening and south-eastward deflection of the flow, at the westward side of the South Atlantic subtropical high due to the Andes mountains. The atmospheric dynamics drive moisture from tropical to extratropical latitudes and contribute to developing convective systems in the austral warm season [39,40]. Bonner (1968) [41] designed an objective procedure to document the occurrence of a low-level jet based on observed wind speed profiles. The procedure considers a range of possible heights at which maximum wind should occur (between 1 and 1.5 km) with three criteria determining maximum intensities and wind-speed dropoffs above those maximums.

Paegle (1998) [42] raised the role of SALLJ in the dispersion of biogeochemical species. SALLJ acts as a conveyor belt in the regional transport of biomass-burning products that impact distant downwind receptors in SESA and the Atlantic Ocean [43,44]. This occurs during the tropical dry season (from June to October) and corresponds to midlatitudes in late austral winter and spring. Owing to this dynamic situation, different SALLJ types

are found according to the region where the jet core is located [45,46]. Particularly, the events that stretch from tropical—about 15° S—to middle latitudes—at least 35° S—with a northwest–southeast orientation are known as Chaco Jet (CJ). The other two types are the No Chaco Jet (NCJ) and the Argentine low-level jet (ALLJ). The configuration of these events meets the SALJ criteria, but the region where it occurs varies. During an NCJ event, the wind is more zonal than meridional, while with CJs the meridional component is the most important. Convection tends to develop between northern Paraguay and southern Brazil. The ALLJ events, develop along the western periphery of a post-frontal anticyclone. In these cases, in contrast to the CJs and NCJs, the main source of moisture is the Atlantic Ocean. Precipitation develops along the eastern slopes of the Andes, in central and northwestern Argentina. The additional requirement of no rain occurring in their span—thus avoiding the wet removal mechanisms—was expected to favor pollen transport from the source region to SESA. Castañeda and Ulke (2015) [47] particularly studied CJs that match this requirement (known as CJ1 events), which represent almost 36% of the total summer variance.

Vertical circulation associated with high- and low-pressure systems, ridges, and troughs plays a crucial role in pollen grain suspension, long-distance transport, and deposition. High-pressure systems are characterized by descending air (subsidence), resulting in fair weather conditions. In contrast, low-pressure systems involve rising air, leading to cloud formation and potential precipitation. Ridges and troughs are wave-shaped pressure systems where horizontal winds circulate anticyclonically and cyclonically. Along the frontal boundaries of ridges, high-pressure regions feature sinking air that promotes fair weather. Instead, upward air motion induces cloudiness and precipitation along trough fronts, conducting atmospheric washout. Updraft and downdraft air movements are quantified by a meteorological variable known as omega. Usually calculated at a 700 hPa geopotential height, omega units are given in Pa s^{-1} , which take positive or negative values. Positive values show air descent, while negative ones air ascent.

3. Material and Methods

3.1. Airborne Pollen Sampling

Atmospheric pollen monitoring was carried out in two periods (1 August 2012–27 November 2012; 9 August 2013–5 December 2013) including the greatest palynological richness in the air of most of the localities studied in Argentina [48]. The survey was performed with a Hirst (1952) [49] seven-day volumetric suction sampler located approximately 3 km SW of Sunchales City, at the National Weather Service station (30°57′24.5″ S, 61°31′59.2″ W, 93 m a.s.l.). The site was selected considering the possibility of capturing subtropical and midlatitude circulation. The device collects the aerosols by inertial impact on an adhesive tape mounted on a drum that spins at a speed of 2 mm h^{-1} . The trap was operated at a constant suction volume of $0.6 \text{ m}^3 \text{ h}^{-1}$. Pollen collection started at 13 UTC; therefore, the “pollen day” lasted from 13 UTC (−3 GMT) day 0 to 12 UTC day + 1. The date assigned to each sample corresponds to day 0. The sticky tape and the slides were prepared by standard techniques [50]. Pollen counting was performed with an optical microscope with a final magnification of 1000×, analyzing the complete slide for each day and seeking the specific pollen types selected in the survey. Observed pollen types were identified using dichotomous keys and images from pollen atlases [51–54] and are expressed as daily concentrations (grains m^{-3} of air). Pollen morphology, the nature of the aerobiological samples, and mineral dust on slides precluded taxonomic determination to the species level using standard light microscopy techniques.

We selected pollen from *Alnus*, *Podocarpus*, and *Nothofagus* to follow subtropical and midlatitude circulations of southern South America. As daily concentrations of these pollen types far from the source are extremely diluted, the data are expressed as the number of pollen grains per 100 cubic meters of air ($\text{gr} \times 100 \text{ m}^{-3}$). Being anemophilous, these pollen types were adapted to air transport and produced in large quantities, making them ideal airborne pollen tracers. In addition, these types of pollen have been previously recorded in

the air from different locations far from their sources, where their presence has been linked to medium- and long-range transport [27,55,56]. *Alnus* (*Alnus acuminata*) grows within the Yungas forest on the eastern slopes of the Andes and Bolivian southern Altiplano in the montane forest vegetation belt between 1600–2700 m a.s.l. [57,58]. Its southernmost geographical distribution reaches 29° S (Catamarca Province, Argentina). *Podocarpus* represents two species: *P. nubigena* from the Subantarctic forests and *P. parlatorei* from the Yungas forest; therefore, it is potentially a tracer for both, midlatitude and subtropical circulation. The genus *Nothofagus* comprises several species (*N. dombeyi*, *N. obliqua*, *N. pumilio*, *N. alessandri*, *N. alpina*, *N. antarctica*, *N. betuloides*, *N. glauca*, *N. macrocarpa*, and *N. nitida*) that grow in South American Subantarctic forests, within a narrow longitudinal strip on the Andes (35.7–55° S), between 500–1800 m a.s.l. at their northern distribution and from sea level up to 500 m a.s.l. on their southernmost location [57,59].

3.2. Meteorological Data and Calculation of Backward Trajectories

Once pollen tracer concentrations were obtained, we sought a connection with their potential sources. Therefore, the online version of the HYSPLIT 4.9 model (Hybrid Single-Particle Lagrangian Integrated Trajectory) of the Air Resources Laboratory (ARL), National Oceanic and Atmospheric Administration (NOAA) [60,61], was used to calculate three-dimensional backward trajectories arriving at Sunchales. Stein et al. (2015) [62] made a complete revision of the historical evolution and multiple applications over the three decades of this model. ARL–Global Data Assimilation System (GDAS) data with a $1^\circ \times 1^\circ$ horizontal resolution were used to perform 72 h backward trajectories covering each pollen day. We considered two arrival heights (750 and 1500 m above ground level) at the synoptic times 00, 06, 12, and 18 UTC. Among the options to compute the vertical pollen transport, we chose the vertical velocity provided by the model. For each trajectory, we checked that no precipitation occurred along the path. In addition, surface meteorological data (daily precipitation, maximum and minimum temperatures, hourly temperature, pressure, present weather, wind speed, and direction) measured at Sunchales Airfield station (National Weather Service) were checked at the time of arrival of the pollen tracers.

Aiming to identify the synoptic systems driving the airborne pollen transport and their evolution, we analyzed the geopotential height (925 and 700 hPa) and vertical pressure velocity (omega 700 hPa) fields for each pollen day. These levels were chosen as representatives of near-surface and mid-tropospheric flow that have been identified as relevant for airborne pollen transport [28]. Study cases representing the most frequent synoptic patterns associated with long-range pollen transport were selected for a detailed description.

For the subtropical circulation, we sought to identify low-level jet situations. The Bonner procedure was adapted to use different meteorological fields (analysis, forecasts, and reanalysis) allowing its application to the extended territories of South America where there are scarce upper air measurements [63]. The modified Bonner's criteria were applied to 850 and 700 hPa GDAS wind fields of the National Center for Environmental Prediction (NCEP). Six hourly fields with one-degree horizontal resolution were considered because of the variations in the synoptic weather conditions and the influence of the daily cycle. Aiming to focus on the airflow structure in the near-source region, the 750/800 hPa layer mean horizontal flow, wind vector, and streamline patterns were studied. In addition, wind vector and omega vertical cross sections were analyzed at the source (19° S) and receptor (30.97° S) latitudes for the start and end times of the transport event, respectively.

The South American midlatitude circulation is dominated by transient synoptic systems moving from SW to NE. We used ERA5 (fifth generation ECMWF reanalysis) gridded data with a regular 0.25° lat–long resolution to obtain the time evolution of 700 hPa geopotential and omega along two different SW–NE transects connecting the *Nothofagus* and *Podocarpus* source region with Sunchales. The information summarized in Hovmöller diagrams allowed us to identify weather systems and their associated horizontal and vertical displacements.

4. Results

4.1. Pollen Tracers of Subtropical Circulation

No trajectory linked the presence of *Podocarpus* with the source located in the Yungas forest. Therefore, *Alnus* was the only tracer analyzed for the subtropical circulation transporting pollen species toward Sunchales.

The backward trajectories show that 35 out of 61 *Alnus* occurrences at Sunchales (57%) are linked with the source location. Nevertheless, considering the flowering period, which extends from August to September, the percentage rises to 64%. Few occurrences (four cases) lay outside these months, but none of them was related to source emission.

The arrival of *Alnus* pollen occurs with a weak cyclonic system (trough or low) located northeast of Sunchales, and the South Atlantic High advanced over the continent (77% of the registered cases; see Table 1). The post-frontal high produces the required air descent for pollen capture.

Table 1. Frequencies of transient synoptic systems (925 hPa geopotential height field) and omega (700 hPa) on the *Alnus* pollen capture dates at Sunchales.

Synoptic Pattern ¹	2012	2013	Percentage
Leading-edge trough	0	2	5.6
Trough-eastern high	7	6	37.0
Low-eastern high	7	7	40.0
Weak high	0	3	9.0
Eastern high	0	1	2.8
Weak low	1	0	2.8
Ridge	0	1	2.8
Total	15	20	100
Omega	2012	2013	Percentage
$\omega > 0$ (descent)	13	13	74.2
$\omega < 0$ (ascent)	2	7	25.7
Total	15	20	100

¹ We provide a cartoon for each pattern in Appendix A, (Figure A1).

The median pollen concentration for the study period was $10 \text{ gr} \times 100 \text{ m}^{-3}$. The highest values (21 and $42 \text{ gr} \times 100 \text{ m}^{-3}$) occurred on 31 August and 1 September 2013 within an episode of continuous arrival that began on 28 August and lasted until 7 September. Therefore, they were selected for a detailed analysis.

Alnus Case Study

Most of the trajectories ending between 14 UTC on 31 August and 12 UTC on 1 September 2013 (Figure 1) start moving towards the northwest and then turn to the southeast when they reach the northern limit of the Yungas forest in southern Bolivia. From this position onward, the trajectories continue in a southerly direction at altitudes between 1000 and 2000 m a.s.l. Travel times take from 28 to 72 h.

The examples in Figure 1 started from 29 to 31 August and ended from 31 August to 1 September. The trajectories illustrate the typical pathway of low-level flow in an SALLJ event. Most of them indicate that air masses travel over the Yungas region, thus advecting pollen southwards. Light-colored ones show how the northerly flow is progressively constrained to the eastern flank of the Andes, while the dark ones (17 UTC 31 August, and 02–18 UTC 1 September) surpass the geographical distribution of the Tucumano–Bolivian Yungas (Figure 1). Near the destination, the trajectories rotate counterclockwise due to the advance of a cold front and arrive at their target location from the south.

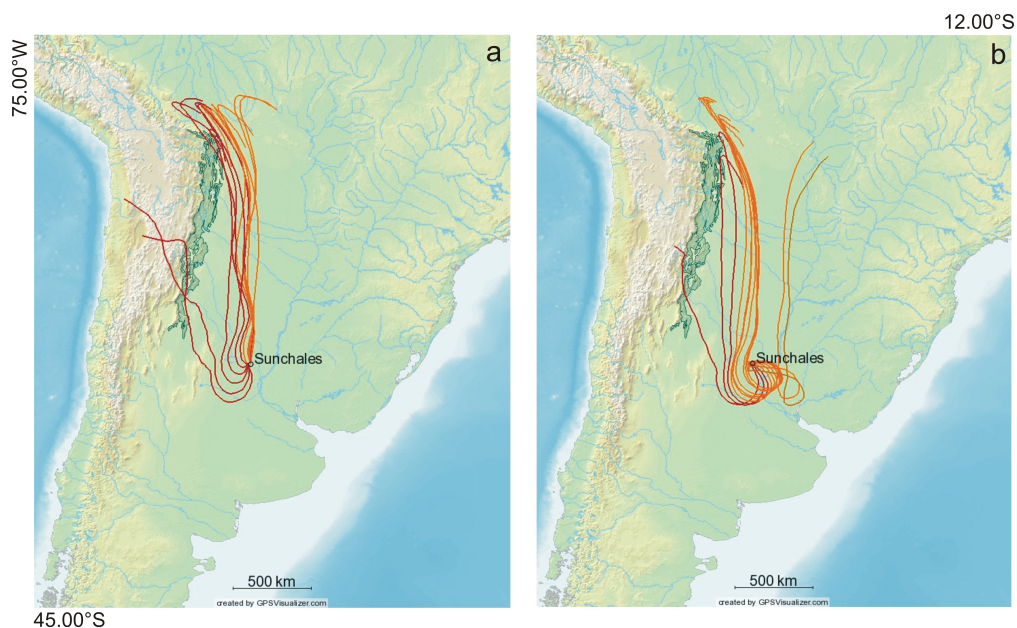


Figure 1. (a) Even-hour *Alnus* trajectories arriving at 1500 m a.s.l. from 14 UTC of 31 August–12 UTC of 1 September 2013 and (b) 14 UTC of 1 September–12 UTC of 2nd September 2013. The Yungas Forest is shaded in green.

The meteorological conditions recorded at Sunchales Aero station show that on 31 August clear skies and low relative humidity (on average 52%) prevailed. The maximum and minimum temperatures reached 32.8 °C and 6.6 °C at 19 UTC and 10 UTC, respectively. On 1 September, surface conditions were similar, with maximum and minimum temperatures of 31.2 and 10.5 °C. Consistent with the calculated trajectories, on 31 August, the wind blew from the north until it changed to a slight southerly wind that increased from 1.2 to 3.1 m s⁻¹ on 1 September.

The synoptic situation remained similar between 31 August and September 1st. The average geopotential height field at 1000 hPa (Figure 2) shows a thermal-induced low-pressure system identified as the Chaco low [64] centered at 25° S, 63° W.

There is an intensified pressure gradient on its eastern flank due to the presence of the South Atlantic Anticyclone over the continent. This feature favors an intense northern meridional component of the wind between the Argentina–Paraguay border. In turn, the midlatitude baroclinic zone is positioned south of 35° S. The 500/1000 hPa thickness field shows a warm air mass (thickness higher than 5700 gpm) over the Amazon basin and northern Argentina. Cold air masses extend up to approximately 40° S (thickness lower than 5400 gpm).

This pattern agrees with the structure described by some authors during an SALLJ event [65,66]. In total, 60% of the analyzed cases were consistent with the no precipitation pattern of CJ1 described by Castañeda and Ulke (2015) [47], while 30% with NCJ and 10% with ALLJ. Moreover, the area that includes central Bolivia, northern Argentina, and Paraguay satisfies the modified Bonner's criteria and presents winds with an intense southward meridional component. Two examples are shown in Figure 3.

The example in Figure 3a shows NNW winds blowing from the source area towards Sunchales, reaching approximately 35° S. The situation on 31 August shows that the jet core moved slightly towards the northeast pushed by the advance of a cold front (Figure 3b).

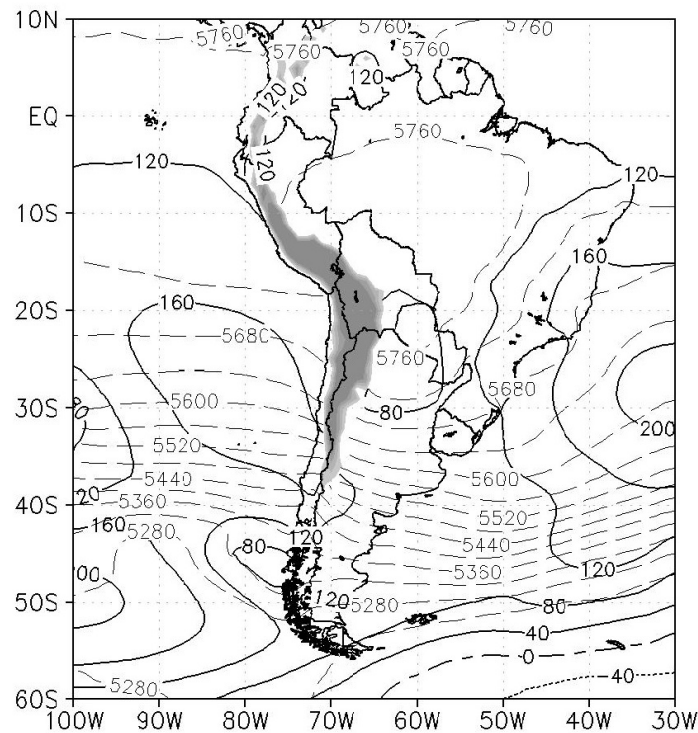


Figure 2. Mean geopotential height at 1000 hPa (black solid lines) and 500/1000 hPa thickness fields (gray dashed lines) for the *Alnus* case study (31 August–1 September 2013). The shaded area shows the highest heights of the Andes (above 1500 m a.s.l.).

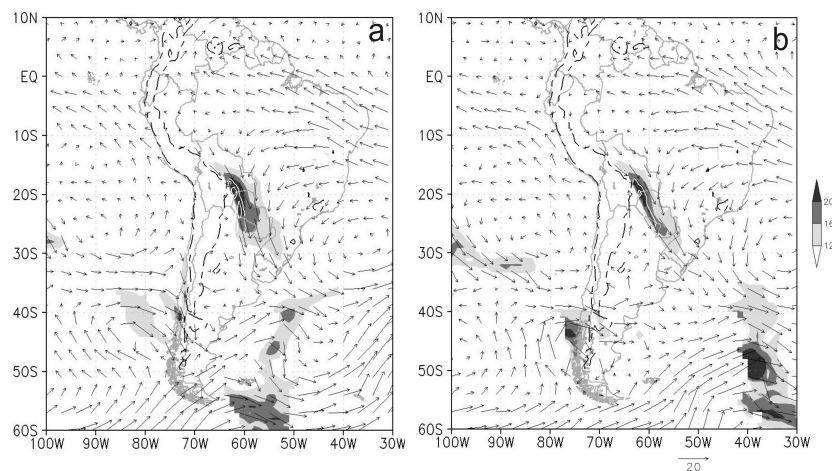


Figure 3. Images of 850 hPa winds (vectors, m s^{-1}) and areas satisfying the modified Bonner's criteria for (a) 06 UTC 31 August and (b) 06 UTC 1 September showing the position of the cold front. Shading indicates wind speeds at 850 hPa greater than 12, 16, and 20 m s^{-1} . White contours indicate a 700/850 hPa wind difference greater than 6, 8, and 10 m s^{-1} . Dashed line masks altitudes above 1500 m.

The streamlines in Figure 4 show a more detailed view of the flow pattern and progression features. The jet core is located over southern Bolivia and northern Paraguay. In addition, the exit region appears in NE Argentina and SE Brazil on 31 August (Figure 4a) with a clear dominance of northern winds over Sunchales. Interestingly, the flow, oriented west to east, overpasses the Yungas region to end up in the jet, thus ensuring the fast advection southwards. The advance of the cold front that extends in the SSE–NNW direction on 1 September (Figure 4b) allows the entry of wind from the south sector towards the central region of Argentina.

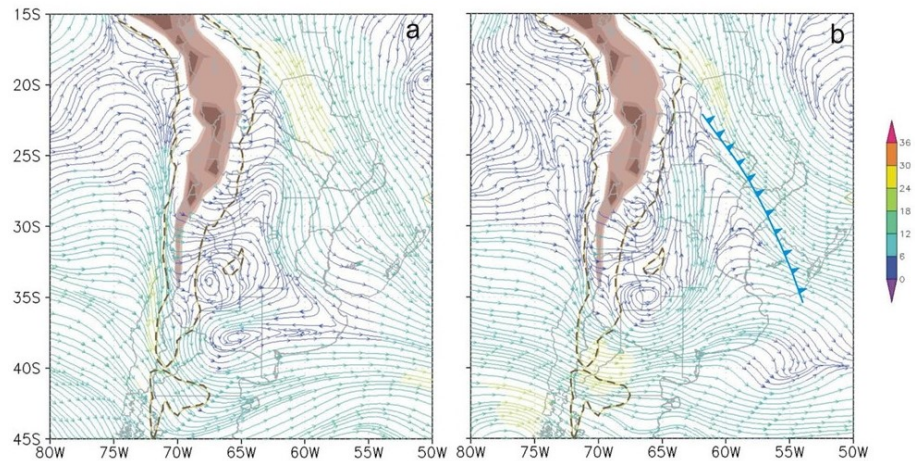


Figure 4. Images of the 800–750 hPa layer mean flow for 06 UTC 31 August (a) and 06 UTC 1 September showing the position of the cold front (b). The dashed line marks the 1500 m altitude, while the shaded area masks altitudes higher than 3250 m. The color scale shows the horizontal wind intensity (m s^{-1}).

The vertical cross sections by the time the studied trajectories arrive at Sunchales show that, until 06 UTC on 31 August, and eastward of the Andes, the wind is predominantly from the north sector except at upper levels where a progressive coupling with the westerlies is observed (Figure 5).

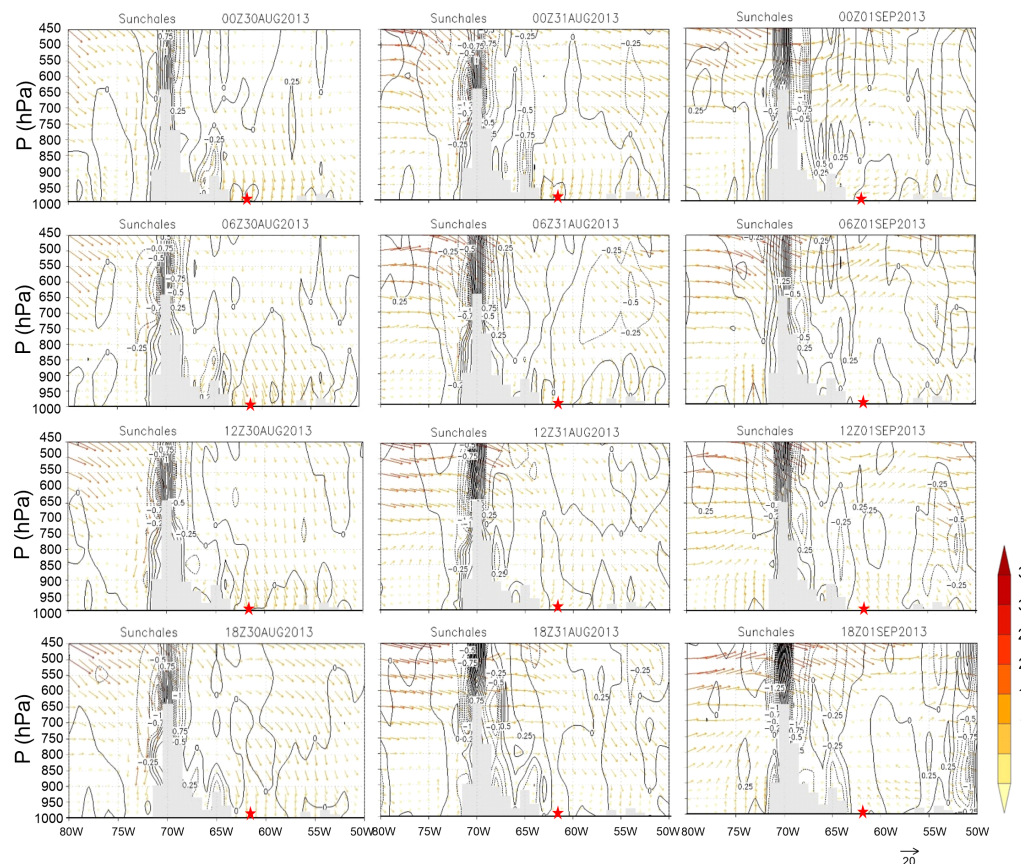


Figure 5. Vertical cross sections (30.97°S) showing the horizontal wind (vectors, m s^{-1}) and omega (lines, Pa s^{-1}) by the end of the SALLJ event. The star shows the position of Sunchales. Panels show the situation every 6 h from 30 August to 1 September 2013. The shaded area shows the Andes and Córdoba ranges. The star indicates the position of Sunchales.

At 12 UTC, below 900 hPa, the wind begins to rotate northeast and east (00 UTC 1 August) to later settle in the south quadrant below the 750 hPa level due to the cold front passage. The atmospheric conditions over Sunchales show moderate subsidence ($\omega > 0$) throughout the period. The progressive displacement of the SALLJ towards the east is also observed.

Figure 6 shows the vertical cross section at the beginning of the event at the latitude of the Yungas. The event starts on 29 August, with no jet structure in the pollen source area. The next day, the wind intensify on the eastern flank of the Andes and ω changes to increasingly negative values (ascents), which is maximum at the time of greater warming (18 UTC, 2:00 p.m. local time).

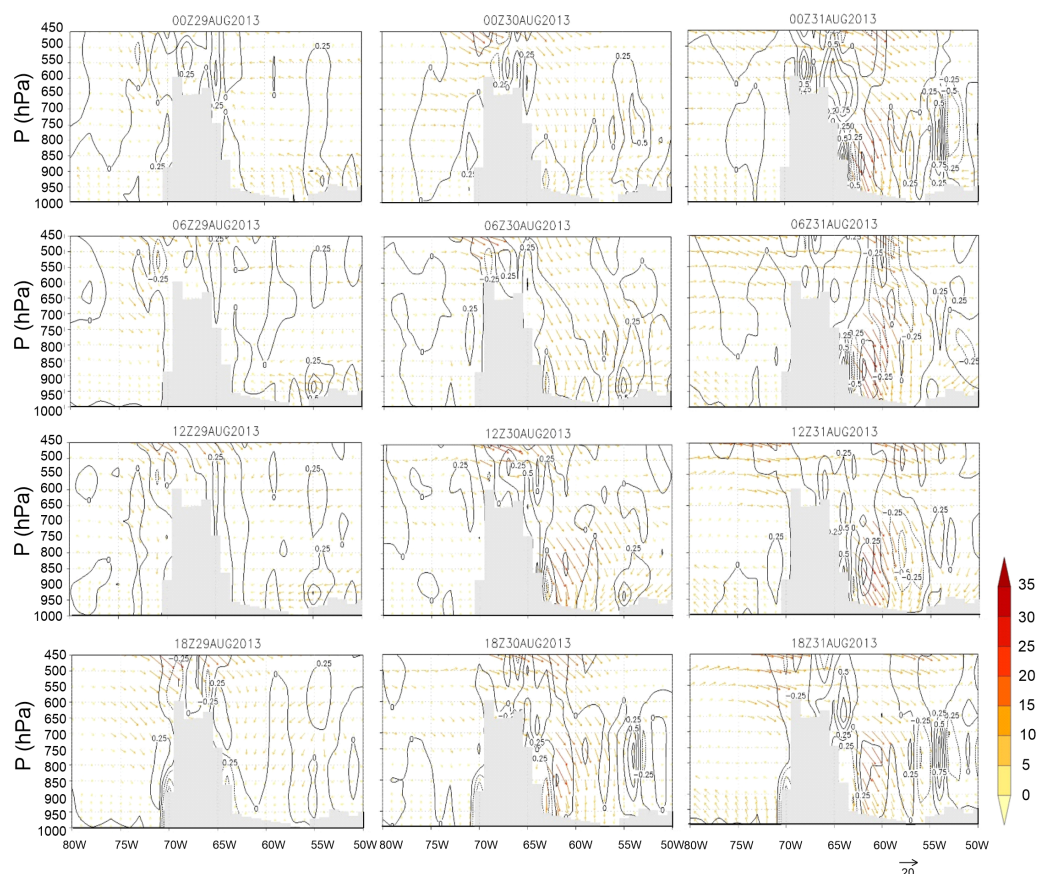


Figure 6. Vertical cross sections (19° S) showing the horizontal wind (vectors, m s^{-1}) and omega (lines, Pa s^{-1}) at the latitude where the SALLJ passes over the Yungas. Panels show the situation every 6 h from 29 August to 31 August 2013 when the event started. The shaded area shows the Andes and Brazilian ranges.

From 12 UTC onward, a wind maximum from the NNW direction and SALLJ characteristics were established below 700 hPa at approximately 62° W. In addition, a positive omega cell is located where the higher wind occurs. The subsidence occurred by the horizontal divergence at the northward inlet of the jet. 31 August is the day of greatest development when the SALLJ core registered NNW winds with more than 20 m s^{-1} . The pattern and values are consistent with those documented by Salio et al. (2007) [67], and Nicolini and García Skabar (2011) [68].

4.2. Pollen Tracers of Midlatitude Circulation

Backward trajectories confirmed that 15 out of 20 *Nothofagus* occurrences at Sunchales (75% of the total cases) linked the source and destination and occurred within the flowering season (October–November). These cases show that the arrival of airborne pollen mainly

occurred with anticyclonic conditions and air subsidence (80% of the cases). Post-frontal features are the most frequent synoptic situations (46.6%, Table 2).

Table 2. Frequencies of transient synoptic systems (700 hPa geopotential height field) and omega (700 hPa) observed at Sunchales on the capture dates of airborne *Nothofagus* pollen.

Synoptic Pattern ¹	2012	2013	Percentage
Leading-edge trough	0	1	6.7
Trough	0	1	6.7
Post-frontal	6	1	46.6
Low	0	1	6.7
Ridge	0	1	6.7
High	1	3	26.6
Total	7	8	100
Omega	2012	2013	Percentage
$\omega > 0$ (descent)	0	3	20
$\omega < 0$ (ascent)	7	5	80
Total	7	8	100

¹ A cartoon for each pattern in Appendix A, (Figure A1).

Similarly, 12 out of 15 total occurrences of *Podocarpus* pollen were linked to the southern source by backward trajectories. Their arrival is mainly related to anticyclonic conditions and air subsidence (75% of total cases) and like the previous case, post-frontal situations are the most frequent (66.7%, Table 3).

Table 3. Frequencies of transient synoptic systems (700 hPa geopotential height field) and omega (700 hPa) observed at Sunchales on the capture dates of airborne *Podocarpus* pollen.

Synoptic Pattern ¹	2012	2013	Percentage
Leading-edge trough	0	3	25.0
Post-frontal	4	4	66.7
High	1	0	8.3
Total	5	7	100
Omega	2012	2013	Percentage
$\omega > 0$ (descent)	0	3	25
$\omega < 0$ (ascent)	5	4	75
Total	5	7	100

¹ Cartoons for each pattern in Appendix A, (Figure A1).

Both *Nothofagus* and *Podocarpus* airborne pollen concentrations were low. They reached medians of $7 \text{ gr} \times 100 \text{ m}^{-3}$ of air and maximum concentrations of 42 and $14 \text{ gr} \times 100 \text{ m}^{-3}$, on 24 November 2012 and 29 October 2013, respectively. Two case examples were selected for further study: 24 November 2012 for *Nothofagus*, and 24 October 2013 for *Podocarpus*.

4.2.1. Backward Trajectories

Nothofagus trajectories show a SW–NE orientation crossing the northern region of the Subantarctic forest on 22–23 November 2012 at an altitude between 2500 and 3500 m.a.s.l. (Figure 7a).

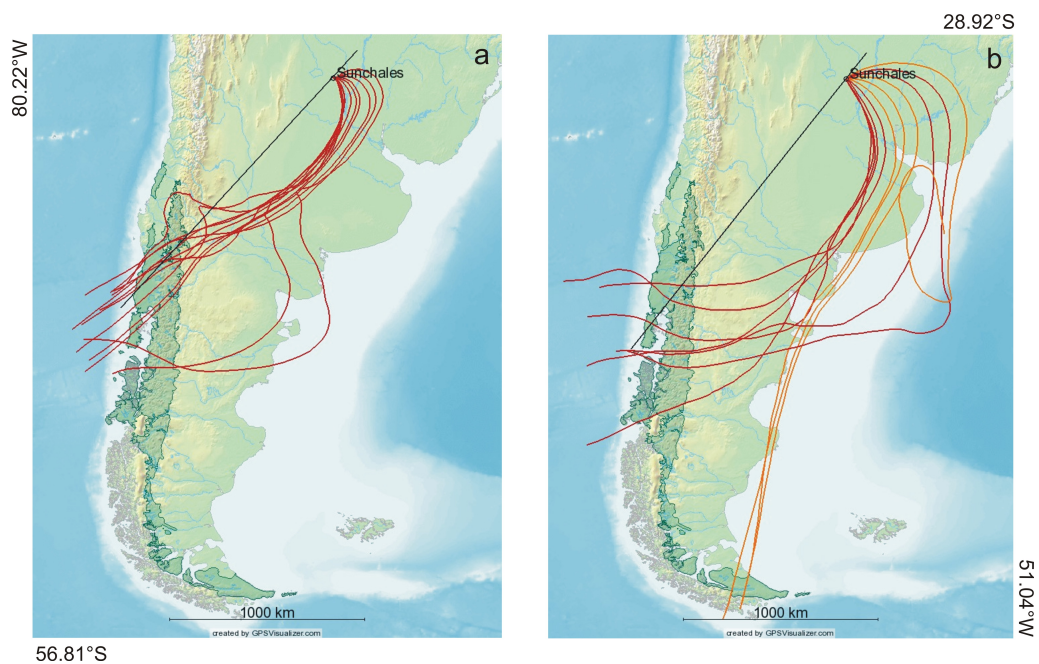


Figure 7. Even-hour *Nothofagus* (a) and *Podocarpus* (b) trajectories arriving at 750 m a.s.l. on 14 UTC of 24 November–12 UTC of 25 November 2012, and 14 UTC 24 October–12 UTC 25 October 2013, respectively. Light-colored lines show trajectories not passing over the pollen source area (see text). Straight lines represent the construction cuts of the Hovmöller diagrams in Figures 8 and 9. The shaded area shows the geographic distribution of the Subantarctic forests.

Podocarpus trajectories crossed the continent at the same latitudinal strip, between 39 and 47° S but with a meridional alignment, and then turned counterclockwise near Sunchales (Figure 7b). The Subantarctic forests were surpassed on 22–23 October 2013 at altitudes ranging from 2000 to 3000 m.a.s.l. Some trajectories passing over the southernmost Subantarctic forest are not linked to the *Podocarpus* pollen source area, as its geographical range only extends between 39.83° and 50.38° S [69]. Also, the curved trajectory (arriving at 12 UTC on 25 October) does not come from the pollen source area. As a rule, the travel time from the source area to the destination point lasts from 48 to 72 h, although in some exceptional cases, they last up to 96 h.

4.2.2. *Nothofagus* Case Study

The Hovmöller diagram in Figure 8 resumes the synoptic situation from 15 November to 1 December 2012 over a transect with a SW–NE orientation (41.54° S, 74.71° W–29.69° S, 60.02° W).

On 16 November, the 700 hPa geopotential field shows a low-pressure system that weakens leeward. Subsequently, between 21 and 22 November, a new trough crosses the Andes range, generating a windward descent over the *Nothofagus* pollen source area. The system moves to the northeast with omega values < 0, which keeps the pollen airborne until the time of arrival (24 November) when the associated subsidence (omega > 0) takes airborne pollen to surface level. On 24 November, clear skies and light winds (2.3 m s^{-1}) predominantly from the SSE direction prevailed at Sunchales. A minimum temperature of 15.1°C was recorded at 10 UTC, while a maximum of 28.4°C was observed at 21 UTC. The mean relative humidity was 62.6%.

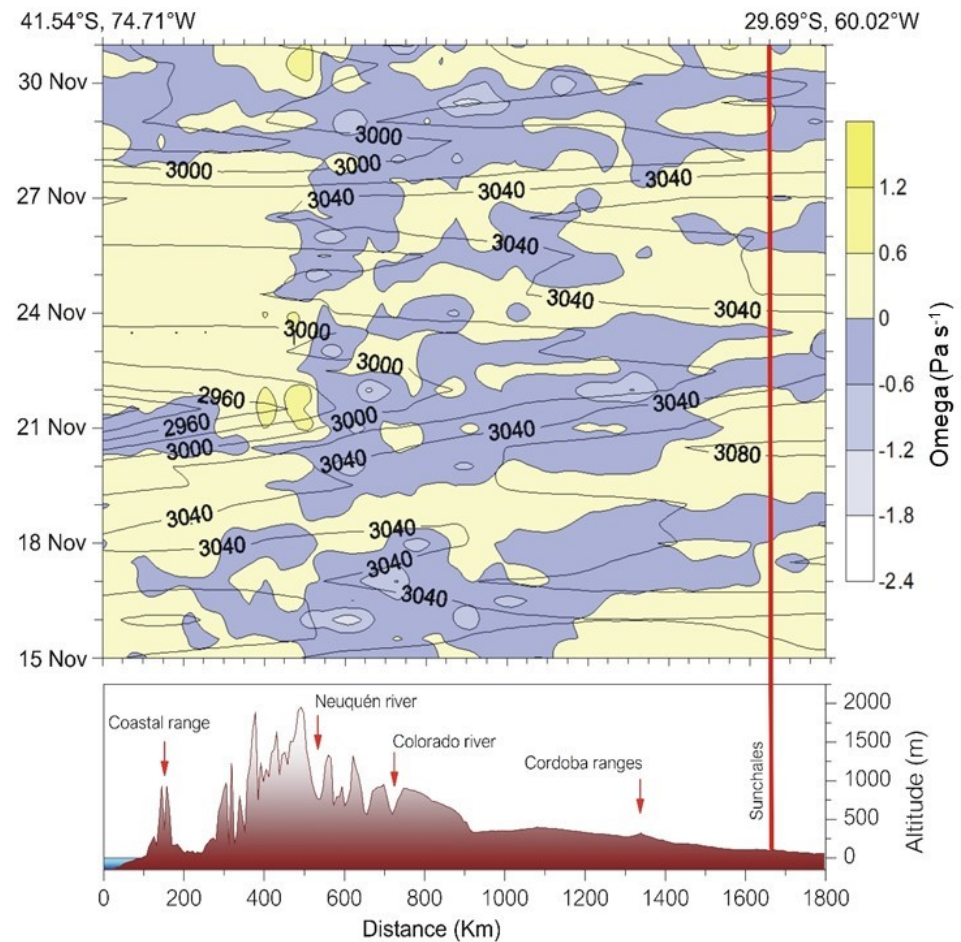


Figure 8. Hovmöller diagram for *Nothofagus* case study from 15 November to 1 December 2012. The space cut corresponds to the straight line in Figure 7a. Lines show the 700 hPa geopotential height (gpm) and the shaded areas show 700 hPa omega (Pa s^{-1}). The lower panel shows the associated topography and the vertical line represents the geographical location of Sunchales.

4.2.3. *Podocarpus* Case Study

The geopotential height field on 22 October 2013 shows a trough passage over the pollen-source area in the Andes of Northern Patagonia (Figure 9). The trough front produces the pollen uplift that enters the free atmosphere to be transported over long distances.

On 23 October, the trough reached Sunchales leading to post-frontal subsidence and the entry of *Podocarpus* pollen to the city on 24 October, when the daily pollen concentration reached $14 \text{ gr} \times 100 \text{ m}^{-3}$. The surface pressure showed a sharp decrease of up to 995 hPa without any significant meteorological phenomena, except for dust due to wind gusts recorded between 20 UTC on 23 October and 01 UTC on 24 October. The 24 October showed clear skies and strong southerly winds (6.3 m s^{-1}). The minimum temperature reached $14.1 \text{ }^\circ\text{C}$ at 10 UTC, while the maximum temperature ($24.7 \text{ }^\circ\text{C}$) occurred at 19 UTC. Also, this day registered the lowest relative humidity of the week (51.6%). Figure 9 also shows a situation similar to that previously described, which occurred between 20 and 22 October, bringing a *Podocarpus* pollen concentration of $7 \text{ gr} \times 100 \text{ m}^{-3}$ to the city.

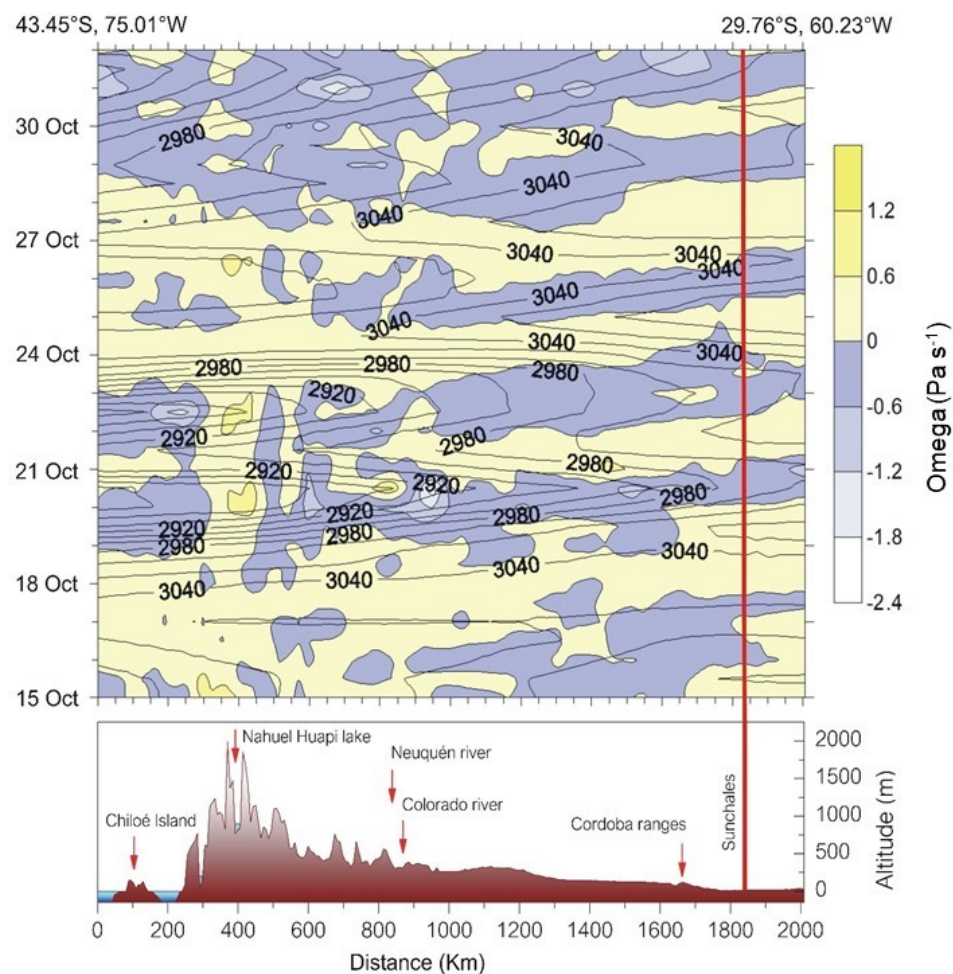


Figure 9. Hovmöller diagram for *Podocarpus* case study from 15 October to 1 November 2013. The space cut corresponds to the straight line in Figure 7b. Lines show the 700 hPa geopotential height (gpm), and shaded areas show 700 hPa omega (Pa s^{-1}). The lower panel shows the associated topography and the vertical line represents the geographical location of Sunchales.

5. Discussion

The *Alnus* geographical distribution represents a pattern of several regions of more or less isolated populations along the eastern flank of the Andes. Today, it reaches approximately 29° S resulting from the complex migration dynamics of repeated glacial–interglacial events during the last million years through Central America from the Northern to the Southern Hemisphere [70–72]. Most of the events of *Alnus* pollen arrival (64% within its flowering period) were linked with a source location, which extended from Jujuy province (Argentina) to the eastern flank of the Bolivian altiplano. Only four cases were not connected with any source location. The absence of other *Alnus* tree species growing in the vicinity of the city of Sunchales presupposes that the source of this tracer is located in the montane forest between 1500 and 2800 m. a.s.l. The analyzed cases show trajectories passing over the southeast of Bolivia and turning to a southerly direction. Afterward, a cold frontal passage rotates trajectories counterclockwise until arrival at Sunchales. Travel times range from 28 to 72 h according to wind intensities. The synoptic situation corresponds to a trough (37%) or weak low (40%) over the source region combined with a high in southeast Brazil. This is consistent with the structure of CJ1 with no precipitation (60%) described by Castañeda and Ulke (2015) [47]. Composite wind fields at 850 hPa indicate that the region meets modified Bonner’s criteria, confirming the presence of a Low-Level Jet east of the Andes. Other SALLJ types were minimally represented in this study. It is important to note that these percentages are significantly influenced by the sampling design. The selection

of airborne pollen sampling sites depends on the specific objectives of the research. The Sunchales location is justified by the SALLJ's role in supplying moisture to the region's agricultural productive core of SESA, thereby enhancing the representation of CJ1 events south of 30° S. Future studies should consider additional sampling locations to thoroughly assess pollen transport across different types of SALLJ, including the NCJ and ALLJ.

Our results show that during its approach to the eastern flank of the Andes, the core of the SALLJ is located at similar altitudes to those at which pollen sources grow, although some kilometers to the east (see Figure 6). The scale of the meteorological analyses of this work does not allow us to explain how the pollen emitted by the source enters the SALLJ. However, streamline results (Figure 4) show an eastward zonal transport up to 6 m s⁻¹ that could account for the entry of pollen into the SALLJ. Previous studies on pollen transport in the Yungas of Jujuy showed mountain–valley breeze systems that produce *Alnus acuminata* upslope transport, up to 3800 m a.s.l. [73]. Presumably, the presence of these mesoscale systems that occur in conditions that favor pollen release may be responsible for this connection.

Concerning pollen source location for *Podocarpus*, no trajectory linked the presence of this pollen type with a northern source, but with the southern one instead. According to Hooghiemstra et al. (2006) [74], the pollen grains from different *Podocarpus* species are morphologically identical; therefore, the detection of this genus does not allow an unambiguous source identification. *P. nubigena* grows in Subantarctic forests, while *Podocarpus parlatorei* grows in the Yungas. According to Bianchi and Olabuenaga (2006) [75], the flowering period of *P. nubigena* extends from October to December, while it is detected in the air of Patagonian localities until February [76]. *P. parlatorei* blooms in October at the end of the dry season [77]. However, no trajectory is linked with the Yungas, but instead with its southern source (Figure 1b). *P. parlatorei* is a low pollen producer causing low airborne pollen concentrations even near its source [78,79]. Moreover, it is also a shade-tolerant species that makes a sparse low-density understory [80,81]. Therefore, *P. parlatorei* is a weak pollen source, which could explain the lack of northerly pollen trajectories; thus, we conclude that Subantarctic forests are their main source. However, the study period may not be sufficient to evaluate the possibility that the northern source has a greater contribution than detected. In this sense, more extensive studies will be necessary.

The biogeography of *Nothofagus* places it not only in southern South America but also in New Guinea, New Zealand, and eastern Australia. According to some authors, this disjoint distribution comes from the detachment of Gondwana [82], while for others, it would represent a post-Gondwanan irradiation that would have begun between 55 and 40 million years ago [83]. The many species of this genus are also difficult to discern with optical microscopy. Those that grow in New Zealand, New Guinea, and eastern Australia are less probable pollen sources for South American locations. Calculated trajectories confirm this hypothesis following previous studies in southeastern Buenos Aires Province [27].

In the case of the southern circulation, the sequence in the source area associated with a long-distance transport event is always the same regardless of the tracer, i.e., whether it is *Nothofagus* or *Podocarpus*. Post-frontal subsidence at 700 hPa ensures good weather conditions and surface diurnal heating triggers the pollen uplift above the ABL to be transported in the free atmosphere. Previous studies in northern Patagonia indicate that airborne pollen transport (*Podocarpus*) initiates with a trough located over the South Pacific Ocean (41% of the studied cases over 5 years) or with its axis over Patagonia (21%) [55]. At the destination, pollen descent from the upper atmosphere occurs by post-frontal subsidence (46.6 for *Nothofagus* and 66.7% for *Podocarpus* of total cases), situations of a leading-edge trough (25% for *Podocarpus*) or a high (26.6% for *Nothofagus*). This mechanism agrees with that described by Gassmann and Pérez (2006) [27] for the transport of *Nothofagus* reaching southeastern Buenos Aires Province; thus, it should be a valid transport mechanism for any pollen type whose source is found in the Subantarctic forests.

6. Concluding Remarks

The study of long-distance transport is of fundamental interest to many disciplines. The entry of allochthonous pollen outbreaks into a given area is of interest to allergology, especially when it occurs in quantities that can cause widespread symptoms in the susceptible population. Anticipating these events is essential and, therefore, of interest to study pollen forecasting. Knowing the dispersion pathways of bioaerosols such as insects or fungal spores has direct applications in agriculture, for example, to prevent biological invasions and the dispersal of crop diseases. On the other hand, pollen grains preserved in the fossil record are used to study climate changes that affect past vegetation. Many of them investigate the role of the SAMS in the hydrological, dust deposition, and vegetation changes detected mainly in the last 2000 years [84–91]. These interpretations require understanding current pollen–climate relationships with which these reconstructions are produced. Knowledge of the atmospheric patterns that disperse pollen over long distances constitutes the first step in building a tool to provide information on changes in atmospheric circulation in the past and an independent technique to cross-validate the reconstructions obtained particularly for the region of Southeastern South America.

Using wind-borne pollen grains as a research method has advantages and disadvantages. One advantage is that these grains are easily identifiable and can be linked to specific plants, making them distinct from other airborne particles. The geographic distribution of the source plants can help determine their origin, especially if the plants are not widely spread. This method also allows us to gain knowledge from pollen with a low contribution to a pollen assemblage (usually less than 2%), which may not be possible through statistical studies. However, the results heavily depend on the monitoring period, which may not always be long enough. Short monitoring periods can lead to generalizations based on non-recurring conditions. Therefore, it is important to validate the results of these studies with long-term research to establish statistically reliable generalizations of the processes being analyzed.

Author Contributions: Conceptualization, C.F.P., A.G.U. and M.I.G.; funding acquisition, C.F.P. and A.G.U.; methodology and pollen counting, C.F.P.; formal analysis, A.G.U. and M.I.G.; data curation, C.F.P.; writing, C.F.P. and A.G.U.; writing, review and editing, C.F.P. All authors have read and agreed to the published version of the manuscript.

Funding: This research was funded by ANPCyT-Argentina (PICT 2008-1739 given to A.G. Ulke and PICT 2020-SERIE A-00366 given to C.F. Pérez).

Institutional Review Board Statement: Not applicable.

Informed Consent Statement: Not applicable.

Data Availability Statement: The original data presented in the study are openly available in the Repositorio Institucional CONICET Digital at <http://hdl.handle.net/11336/240591> (accessed on 3 September 2024).

Acknowledgments: We appreciate the support of SanCor Cooperativa de Seguros Ltda. which installed the Burkard trap at Sunchales and provided transport logistics for the pollen samples. We would especially like to thank the Sunchales weather station personnel who operate the Burkard trap. Without their collaboration, this work would not have been possible. We gratefully thank the National Weather Service which provided the meteorological data for this study. Figures 1 and 7 were drawn with GPS Visualizer, a free online drawing map website <http://www.gpsvisualizer.com/> (accessed on 3 September 2024).

Conflicts of Interest: The authors declare no conflicts of interest.

Abbreviations

The following abbreviations are used in this manuscript:

SESA	Southeastern South America
SAMS	South American Monsoon System
SALLJ	South American Low-Level Jet
CJ	Chaco Jet
CJ1	Chaco Jet with no precipitation
ALLJ	Argentine low-level jet
NCJ	No Chaco Jet
UTC	Coordinated Universal Time
m a.s.l.	meters above sea level
HYSPLIT	Hybrid Single-Particle Lagrangian Integrated Trajectory model
ARL	Air Resources Laboratory
NOAA	National Oceanic and Atmospheric Administration
GDAS	Global Data Assimilation System
NCEP	National Center for Environmental Prediction

Appendix A

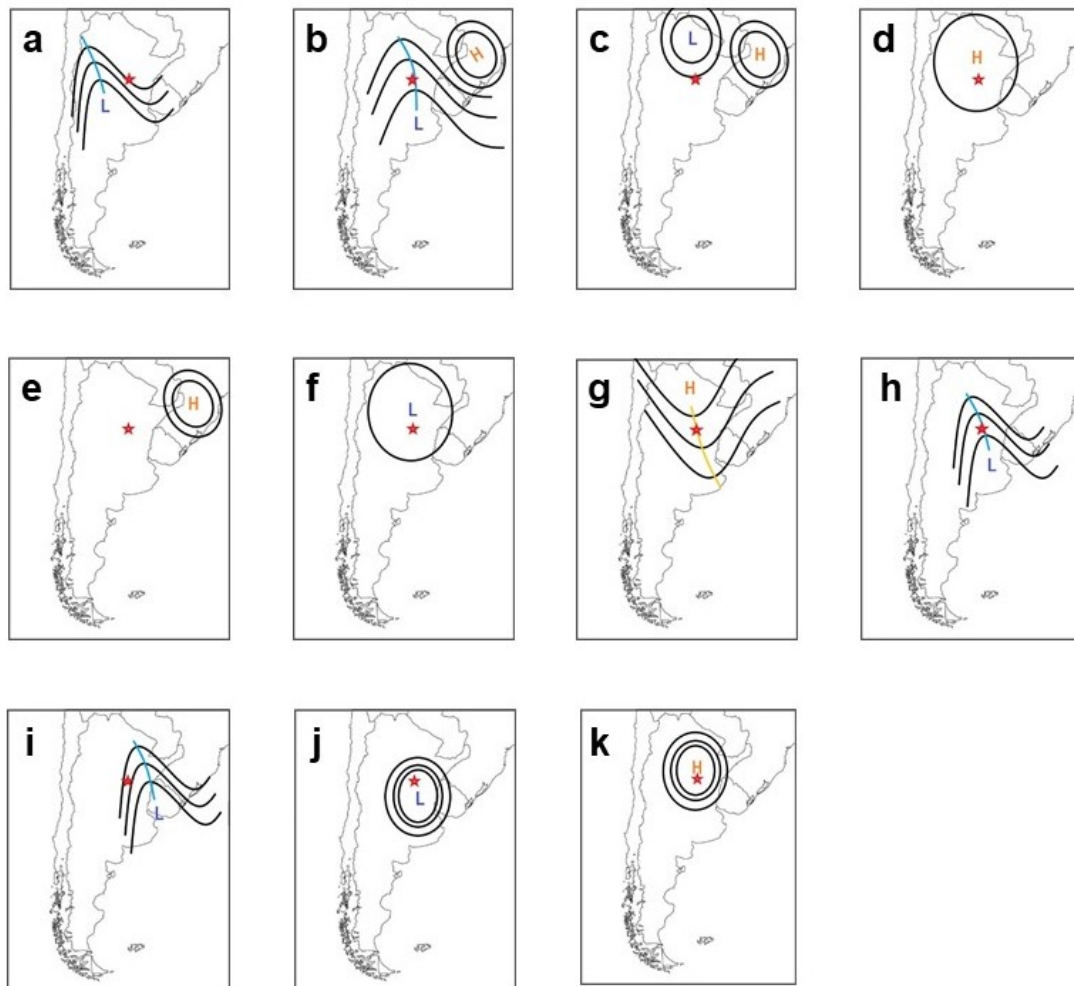


Figure A1. Cartoons describing the transient synoptic patterns (see Tables 1–3) recognized for *Alnus*, *Nothofagus*, and *Podocarpus* pollen arrival at Sunchoales. The red star shows the city’s location. (a) leading-edge trough, (b) trough–eastern high, (c) low–eastern high, (d) weak high, (e) eastern high, (f) weak low, (g) ridge, (h) trough, (i) post-frontal, (j) low, (k) high.

References

1. Prentice, C.I. Pollen representation, source area, and basin size: Toward a unified theory of pollen analysis. *Quat. Res.* **1985**, *23*, 76–86. [[CrossRef](#)]

2. Prentice, C.I. Records of vegetation in time and space: The principles of pollen analysis. In *Vegetation History*; Handbook of Vegetation Science; Huntley, B., Webb, T., Eds.; Springer: Dordrecht, The Netherlands, 1988; Volume 7, pp. 17–42.
3. Sugita, S. A Model of Pollen Source Area for an Entire Lake Surface. *Quat. Res.* **1993**, *39*, 239–244.
4. Sugita, S. Pollen Representation of Vegetation in Quaternary Sediments: Theory and Method in Patchy Vegetation. *J. Ecol.* **1994**, *82*, 881–897. [[CrossRef](#)]
5. Sugita, S. Theory of quantitative reconstruction of vegetation I: Pollen from large sites REVEALS regional vegetation composition. *Holocene* **2007**, *17*, 229–241. [[CrossRef](#)]
6. Sugita, S. Theory of quantitative reconstruction of vegetation II: All you need is LOVE. *Holocene* **2007**, *17*, 243–257. [[CrossRef](#)]
7. Gaillard, M.J.; Sugita, S.; Bunting, M.J.; Middleton, R.; Broström, A.; Caseldine, C.; Giesecke, T.; Hellman, S.E.; Hicks, S.; Hjelle, K.; et al. The use of modeling and simulation approach in reconstructing past landscapes from fossil pollen data: A review and results from the POLLANDCAL network. *Veget. Hist. Archaeobot.* **2008**, *17*, 419–443. [[CrossRef](#)]
8. Hjelmroos, M. Long-distance transport of *Betula* pollen grains and allergic symptoms. *Aerobiologia* **1992**, *8*, 231–236. [[CrossRef](#)]
9. Emberlin, J. The effects of patterns in climate and pollen abundance on allergy. *Allergy* **1994**, *49*, 15–20. [[CrossRef](#)]
10. Cecchi, L.; Morabito, M.; Domeneghetti, M.P.; Crisci, A.; Onorari, M.; Orlandini, S. Long distance transport of ragweed pollen as a potential cause of allergy in central Italy. *Ann. Allergy. Asthma Imm.* **2006**, *96*, 86–91.
11. D’Amato, G.; Cecchi, L.; Bonini, S.; Nunes, C.; Annesi-Maesano, I.; Behrendt, H.; Liccardi, G.; Popov, T.; Van Cauwenberge, P. Allergenic pollen and pollen allergy in Europe. *Allergy* **2007**, *62*, 976–990.
12. Sofiev, M.; Belmonte, J.; Gehrig, R.; Izquierdo, R.; Smith, M.; Dahl, A.; Siljamo, P. Airborne Pollen Transport. In *Allergenic Pollen*; Sofiev, M., Bergmann, K.C., Eds.; Springer: Dordrecht, The Netherlands, 2013; pp. 127–159.
13. Zhang, R.; Duhl, T.; Salam, M.T.; House, J.M.; Flagan, R.C.; Avol, E.L.; Gilliland, F.D.; Guenther, A.; Chung, S.H.; Lamb, B.K.; et al. Development of a regional-scale pollen emission and transport modeling framework for investigating the impact of climate change on allergic airway disease. *Biogeosciences* **2013**, *10*, 3977–4023. [[CrossRef](#)]
14. Skjøth, C.A.; Sommer, J.; Stach, A.; Smith, M.; Brandt, J. The long-range transport of birch (*Betula*) pollen from Poland and Germany causes significant pre-season concentrations in Denmark. *Allergy* **2007**, *37*, 1204–1212. [[CrossRef](#)] [[PubMed](#)]
15. Siljamo, P.; Sofiev, M.; Severova, E.; Ranta, H.; Kukkonen, J.; Polevova, S.; Kubin, E.; Minin, A. Sources, impact, and exchange of early-spring birch pollen in the Moscow region and Finland. *Aerobiologia* **2008**, *24*, 211–230. [[CrossRef](#)]
16. Izquierdo, R.; Belmonte, J.; Avila, A.; Alarcón, M.; Cuevas, E.; Alonso-Pérez, S. Source areas and long-range transport of pollen from continental land to Tenerife (Canary Islands). *Int. J. Biometeorol.* **2011**, *55*, 67–85. [[CrossRef](#)]
17. Després, V.R.; Huffman, J.A.; Burrows, S.M.; Hoose, C.; Safatov, A.S.; Buryak, G.; Fröhlich-Nowoisky, J.; Elbert, W.; Andreae, M.O.; Pöschl, U.; et al. Primary biological aerosol particles in the atmosphere: A review. *Tellus B* **2012**, *64*, 1–40. [[CrossRef](#)]
18. Fraile, R.; Calvo, A.I.; Castro, A.; Fernández-González, D.; García-Ortega, E. The behavior of the atmosphere in long-range transport. *Aerobiologia* **2006**, *22*, 35–45. [[CrossRef](#)]
19. Sofiev, M.; Siljamo, P.; Ranta, H.; Rantio-Lehtimäki, A. Towards numerical forecasting of long-range air transport of birch pollen: Theoretical considerations and a feasibility study. *Int. J. Biometeorol.* **2006**, *50*, 392–402. [[CrossRef](#)]
20. Bourgeois, J.C.; Koerner, R.M.; Alt, B.T. Airborne pollen: A unique air mass tracer, its influx to the Canadian high Arctic. *Ann. Glaciol.* **1985**, *7*, 109–116. [[CrossRef](#)]
21. Rousseau, D.-D.; Duzer, D.; Cambon, G.; Jolly, D.; Poulsen, U.; Ferrier, J.; Schevin, P.; Gros, R. Long-distance transport of pollen to Greenland. *Geophys. Res. Lett.* **2003**, *30*, 1–4. [[CrossRef](#)]
22. Rousseau, D.-D.; Duzer, D.; Etienne, J.-L.; Cambon, G.; Jolly, D.; Ferrier, J.; Schevin, P. Pollen record of rapidly changing air trajectories to the North Pole. *J. Geophys. Res.* **2004**, *109*, 1–7. [[CrossRef](#)]
23. Waisel, Y.; Ganor, E.; Epshtein, V.; Stupp, A.; Eshel, A. Airborne pollen, spores, and dust across the east Mediterranean Sea. *Aerobiologia* **2008**, *24*, 125–131. [[CrossRef](#)]
24. Hernández-Ceballos, M.A.; García-Mozo, H.; Adame, J.A.; Domínguez-Vilches, E.; Bolívar, J.P.; De la Morena, B.A.; Pérez-Badía, R.; Galán, C. Determination of potential sources of *Quercus* airborne pollen in Córdoba city (southern Spain) using back-trajectory analysis. *Aerobiologia* **2011**, *27*, 261–276. [[CrossRef](#)]
25. Celenk, C. Detection of reactive allergens in long-distance transported pollen grains: Evidence from *Ambrosia*. *Atmos. Environ.* **2019**, *209*, 212–219. [[CrossRef](#)]
26. Negral, L.; Moreno-Grau, S.; Galera, M.D.; Elvira-Rendueles, B.; Costa-Gómez, I.; Aznar, F.; Pérez-Badía, R.; Moreno, J.M. The effects of continentality, marine nature and the recirculation of air masses on pollen concentration: *Olea* in the Mediterranean coastal enclave. *Total Environ.* **2021**, *790*, 1–13. [[CrossRef](#)]
27. Gassmann, M.I.; Pérez, C.F. Trajectories associated with regional and extra-regional pollen transport in the southeast of Buenos Aires province, Mar del Plata (Argentina). *Int. J. Biometeorol.* **2006**, *50*, 280–291. [[CrossRef](#)]
28. Pérez, C.F.; Castañeda, M.E.; Gassmann, M.I.; Bianchi, M.M. A statistical study of *Weinmannia* pollen trajectories across the Andes. *Adv. Geosci.* **2009**, *22*, 79–84. [[CrossRef](#)]
29. Pérez, C.F.; Bianchi, M.M.; Gassmann, M.I.; Tonti, N.; Pisso, I. A case study of anisotropic airborne pollen transport in Northern Patagonia using a Lagrangian particle dispersion model. *Rev. Palaeobot. Palynol.* **2018**, *258*, 215–222. [[CrossRef](#)]
30. Meza Torres, E.I.; Cerne, B.; Ulke, A.G.; Morbelli, M.A. Distribution of *Ophioglossum reticulatum* L. in South America. A case of long-distance jump dispersal? *Int. J. Biometeorol.* **2015**, *59*, 137–150. [[CrossRef](#)]
31. Garreaud, R.D. The Andes climate and weather. *Adv. Geosci.* **2009**, *22*, 3–11. [[CrossRef](#)]

32. Compagnucci, R.H.; Salles, M.A. Surface pressure patterns during the year over southern South America. *Int. J. Climatol.* **1997**, *17*, 635–653. [[CrossRef](#)]
33. Garreaud, R.D.; Wallace, J.M. Summertime incursions of midlatitude air into tropical and subtropical South America. *Mon. Weather Rev.* **1998**, *126*, 2713–2733. [[CrossRef](#)]
34. Garreaud, R.D. Cold air incursions over Subtropical South America: Mean structure and dynamics. *Mon. Weather Rev.* **2000**, *128*, 2544–2559. [[CrossRef](#)]
35. Müller, G.V.; Berri, G.J. Atmospheric circulation associated with persistent generalized frosts in Central-Southern South America. *Mon. Weather Rev.* **2007**, *135*, 1268–1289. [[CrossRef](#)]
36. Müller, G.V.; Berri, G.J. Atmospheric circulation associated with extreme generalized frost persistence in central-southern South America. *Clim. Dyn.* **2012**, *38*, 837–857. [[CrossRef](#)]
37. de Carvalho, L.M.V.; Cavalcanti, I.F.A. The South American Monsoon System (SAMS). In *The Monsoons and Climate Change*; de Carvalho, L., Jones, C., Eds.; Springer Climate; Springer: Cham, Switzerland, 2016.
38. Marengo, J.A.; Liebmann, B.; Grimm, A.M.; Misra, V.; Silva Dias, P.L.; Cavalcanti, I.F.A.; Carvalho, L.M.V.; Berbery, E.H.; Ambrizzi, T.; Vera, C.S.; et al. Recent developments on the South American monsoon system. *Int. J. Climatol.* **2012**, *32*, 1–21. [[CrossRef](#)]
39. Nicolini, M.; Saulo, A.C. Modeled Chaco low-level jets and related precipitation patterns during the 1997–1998 warm season. *Meteorol. Atmos. Phys.* **2006**, *94*, 129–143. [[CrossRef](#)]
40. Vera, C.; Baez, J.; Douglas, M.; Emmanuel, C.B.; Marengo, J.; Meitin, J.; Nicolini, M.; Noguez-Paegle, J.; Paegle, J.; Penalba, O.; et al. The South American low-level jet experiment. *Bull. Am. Meteorol. Soc.* **2006**, *87*, 63–78. [[CrossRef](#)]
41. Bonner, W.D. Climatology of the Low Level Jet. *Mon. Weather Rev.* **1968**, *96*, 833–850. [[CrossRef](#)]
42. Paegle, J. A comparative review of South American low-level jets. *Meteorologica* **1998**, *23*, 73–81.
43. Freitas, S.R.; Longo, K.M.; Silva Dias, M.A.F.; Silva Dias, P.L.; Chatfield, R.; Prinsd, E.; Artaxo, P.; Grell, G.A.; Recuero, F.S. Monitoring the Transport of Biomass Burning Emissions in South America. *Environ. Fluid Mech.* **2005**, *5*, 135–167. [[CrossRef](#)]
44. Ulke, A.G. Influence of regional transport mechanisms on the fingerprints of biomass-burning aerosols in Buenos Aires. *Adv. Meteorol.* **2019**, *2019*, 1–13. [[CrossRef](#)]
45. Nicolini, M.; Salio, P.; Borque, P. Thermodynamic and kinematic characterization of the low-level troposphere during SALLJEX in different large-scale environments. In Proceedings of the 8th International Conference on Southern Hemisphere Meteorology and Oceanography, Foz do Iguacu, Brazil, 24–28 April 2006.
46. Salio, P.; Nicolini, M. Seasonal characterization on the diurnal cycle of convection frequency over Southeastern South America under different low-jet conditions. In Proceedings of the 8th International Conference on Southern Hemisphere Meteorology and Oceanography, Foz do Iguacu, Brazil, 24–28 April 2006.
47. Castañeda, M.E.; Ulke, A.G. Analysis of atmospheric conditions associated to CHACO events of the Low Level Jet East of the Andes and their implications for regional transport. *Int. J. Climatol.* **2015**, *35*, 4126–4138. [[CrossRef](#)]
48. Pérez, C.F.; Gassmann, M.I.; Ulke, A.G.; Merino, R. Diversidad polínica atmosférica en la ciudad de Sunchales (Santa Fe, Argentina): Agosto – noviembre 2012, agosto – diciembre 2013. *Bol. Soc. Argent. Bot.* **2020**, *55*, 573–585. [[CrossRef](#)]
49. Hirst, J.M. An automatic volumetric spore trap. *Ann. Appl. Biol.* **1952**, *39*, 257–265. [[CrossRef](#)]
50. Kåpylä, M.; Penttinen, A. An evaluation of the microscopical counting methods of the tape in Hirst-Burkard pollen and spore trap. *Grana* **1981**, *20*, 131–141. [[CrossRef](#)]
51. Heusser, C.J. *Pollen and Spores of Chile: Modern Types of the Pteridophyta, Gymnospermae, and Angiospermae*, 3rd ed.; Univ. Arizona Press: Tucson, AZ, USA, 1971; pp. 154–196.
52. Markgraf, V.; D’Antoni, H.L. *Pollen Flora of Argentina. Modern Spore and Pollen Types of Pteridophyta, Gymnospermae and Angiospermae*, 3rd ed.; Univ. Arizona Press: Tucson, AZ, USA, 1978; pp. 154–196.
53. Pire, S.M.; Anzótegui, L.M.; Cuadrado, G.A. (Eds.) *Flora polínica del Nordeste Argentino. Volumen I*, 3rd ed.; EUDENE-UNNE: Corrientes, Argentina, 1998; p. 143.
54. Pire, S.M.; Anzótegui, L.M.; Cuadrado, G.A. (Eds.) *Flora polínica del Nordeste Argentino. Volumen II*, 3rd ed.; EUDENE-UNNE: Corrientes, Argentina, 2001; p. 172.
55. Pérez, C.F.; Gassmann, M.I.; Bianchi, M.M.; Tonti, N. Airborne pollen transport of *Podocarpus* sp.: The study of backward trajectories and associated synoptic situations. In Proceedings of the 9th International Congress on Aerobiology, Buenos Aires, Argentina, 23–27 August 2010.
56. Pérez, C.F.; Latorre, F.; Ulke, G.; Alonso, C.A. Retro-trayectorias de masas de aire asociadas a la llegada de polen del Bosque Montano de Yungas a la ciudad de Diamante (Entre Ríos). In Proceedings of the Congremet XI, Buenos Aires, Argentina, 28 May–1 June 2012.
57. Oyarzabal, M.; Clavijo, J.; Oakley, L.; Biganzoli, F.; Tognetti, P.; Barberis, I.; Maturo, H.M.; Aragón, R.; Campanello, P.I.; Prado, D.; et al. Unidades de vegetación de la Argentina. *Ecol. Aust.* **2018**, *20*, 40–63. [[CrossRef](#)]
58. Arturi, M.F.; Grau, H.R.; Aceñolaza, P.G.; Brown, A.D. Estructura y sucesión en bosques montanos del noroeste de Argentina. *Rev. Biol. Trop.* **1998**, *46*, 525. [[CrossRef](#)]
59. Luebert, F.; Plischoff, P. *Sinopsis Bioclimática y Vegetacional de Chile*, 3rd ed.; Editorial Universitaria: Santiago, Chile, 2017; pp. 154–196.
60. Draxler, R.R.; Hess, G.D. *Description of the HYSPLIT 4 Modeling System*; NOAA Technical Memorandum ERL ARL224; Air Resources Laboratory: Silver Spring, MD, USA, 1997; 25p.

61. Draxler, R.R.; Hess, G.D. An overview of the HYSPLIT 4 modeling system for trajectories, dispersion and deposition. *Aust. Meteorol. Mag.* **1998**, *47*, 295–308.
62. Stein, A.F.; Draxler, R.R.; Rolph, G.D.; Stunder, B.J.B.; Cohen, M.D.; Ngan, F. NOAA's HYSPLIT atmospheric transport and dispersion modeling system. *Bull. Am. Meteorol. Soc.* **1998**, *96*, 2059–2077. [[CrossRef](#)]
63. Oliveira, M.I.; Nascimento, E.L.; Kannenberg, C. A new look at the identification of low-level jets in South America. *Mon. Weather Rev.* **2018**, *146*, 2315–2334. [[CrossRef](#)]
64. Seluchi, M.E.; Saulo, A.C.; Nicolini, M.; Satyamurty, P. The northwestern Argentinean low: A study of two typical events. *Mon. Weather Rev.* **2003**, *131*, 2361–2378. [[CrossRef](#)]
65. Nicolini, M.; Saulo, C.; Torres, C.J.; Salio, P. Strong South American low-level jet events characterization during warm season and implications for enhanced precipitation. *Meteorol. Spec. Issue S. Am. Monsoon Syst.* **2002**, *27*, 59–69.
66. Salio, P.V. Caracterización de Eventos de Corriente en Chorro en Capas Bajas de la Atmósfera en Base a Reanálisis y la Precipitación Asociada en el Sudeste de Sudamérica. Ph.D. Thesis, Universidad de Buenos Aires, Buenos Aires, Argentina, 2002.
67. Salio, P.; Nicolini, M.; Zipser, E.J. Mesoscale Convective Systems over Southeastern South America and Their Relationship with the South American Low-Level Jet. *Mon. Weather Rev.* **2007**, *135*, 1290–1309. [[CrossRef](#)]
68. Nicolini, M.; Garcia Skabar, Y. Diurnal Cycle in convergence pattern in the boundary layer east of the Andes and convection. *Atmos. Res.* **2011**, *100*, 377–390. [[CrossRef](#)]
69. Marticorena, C.; Rodríguez, R. *Flora de Chile I*; Universidad de Concepción: Santiago, Chile, 1995; 157p.
70. Furlow, J.J. The systematics of the American species of *Alnus* (Betulaceae). Part I. *Rhodora* **1979**, *81*, 1–121.
71. Gómez, L.D. *Vegetación de Costa Rica*; EUNED: San José, Costa Rica, 1986; 327p.
72. Rich, P.V.; Rich, T.H. The Central American dispersal route: Biotic history and paleogeography. In *Costa Rican Natural History*; Janzen, D.H., Ed.; The University of Chicago: Chicago, IL, USA, 1983; pp. 12–34.
73. Torres, G.R.; Pérez, C.F.; Lupo, L.C. Altitudinal patterns of wind transport and deposition of Yungas tree pollen in northwestern Argentina: Implications for interpreting the Quaternary fossil record. *Palaeogeogr. Palaeoclimatol. Palaeoecol.* **2019**, *520*, 66–77. [[CrossRef](#)]
74. Hooghiemstra, H.; Wijninga, V.M.; Cleef, A.M. The paleobotanical record of Colombia: Implications for biogeography and biodiversity. *Ann. Mo. Bot. Gard.* **2006**, *93*, 377–390. [[CrossRef](#)]
75. Bianchi, M.M.; Olabuenaga S.E. A 3-year airborne pollen and fungal spores record in San Carlos de Bariloche, Patagonia, Argentina. *Aerobiologia* **2006**, *22*, 247–257. [[CrossRef](#)]
76. Bianchi, M.M.; Olabuenaga, S.E.; Dzendoletas, M.; Crivelli, E.S. El registro polínico atmosférico de San Carlos De Bariloche: septiembre 2001-septiembre 2002. *Rev. Mus. Argent. Cienc. Nat.* **2004**, *6*, 1–7.
77. Ayma-Romay, A.I.; Sanzetenea, E.S. Variaciones fenológicas de especies de Podocarpaceae en estación seca de los Yungas (Cochabamba, Bolivia). *Ecol. Boliv.* **2008**, *43*, 16–28.
78. García de Albano, M.E. Lluvia polínica en selvas montañas de la provincia de Tucumán, Argentina. *Rev. Mus. Argent. Cienc. Nat.* **2006**, *8*, 159–164. [[CrossRef](#)]
79. García, M.E.; Reyes, N.J.; Espeche, M.L.; Ordano, M.; Lamelas, C.; Forciniti, J.; Gómez, L.S. Strong seasonal effects and long-term weather-related factors drive the temporal variability of airborne pollen in the atmosphere of San Miguel de Tucumán, Argentina. *Grana* **2021**, *60*, 372–384. [[CrossRef](#)]
80. Pinazo, M.A.; Gasparri, N.I.; Goya, J.F.; Arturi, M.F. Caracterización estructural de un bosque de *Podocarpus parlatorei* y *Juglans australis* en Salta, Argentina. *Rev. Biol. Trop.* **2003**, *51*, 361–368. [[PubMed](#)]
81. Quiroga M.P.; Premoli, A.C. El rol de las poblaciones marginales en la conservación del acervo genético de la única conífera del sur de Yungas en Argentina y Bolivia, *Podocarpus parlatorei* (Podocarpaceae). *Ecol. Boliv.* **2013**, *48*, 4–16.
82. Swenson, U.; Hill, R.S.; McLoughlin, S. Biogeography of *Nothofagus* supports the sequence of Gondwana break-up. *Taxon* **2001**, *50*, 1025–1041. [[CrossRef](#)]
83. Lyn, G.C.; Michael, D.C. Not so ancient: The extant crown group of *Nothofagus* represents a post-Gondwanan radiation. *R. Soc. Biol. Biol. Sci.* **2005**, *272*, 2535–2544.
84. Piovano, E.L.; Ariztegui, D.; Córdoba, F.; Cioccale, M.; Sylvestre, F. Hydrological Variability in South America below the Tropic of Capricorn (Pampas and Patagonia, Argentina) during the last 13.0 Ka. In *Past Climate Variability in South America and Surrounding Regions. Developments in Paleoenvironmental Research*; Vimeux, F., Sylvestre, F., Khodri, M., Eds.; Springer: Dordrecht, The Netherlands, 2009; Volume 14.
85. Troin, M.; Vallet-Coulomb, C.; Sylvestre, F.; Piovano, E. Hydrological modelling of a closed lake (Laguna Mar Chiquita, Argentina) in the context of 20th century climatic changes. *J. Hydrol.* **2010**, *393*, 233–244. [[CrossRef](#)]
86. Hooper, J.; Marx, S.K.; May, J.H.; Lupo, L.C.; Kulemeyer, J.J.; Pereira, E.D.L.Á.; Seki, O.; Heijnis, H.; Child, D.; Gadd, P.; et al. Dust deposition tracks late-Holocene shifts in monsoon activity and the increasing role of human disturbance in the Puna-Altiplano, northwest Argentina. *Holocene* **2020**, *30*, 519–536. [[CrossRef](#)]
87. Jara, I.A.; Maldonado, A.; de Porras, M.E. Late Holocene dynamics of the South American summer monsoon: New insights from the Andes of northern Chile (21° S). *Quat. Sci. Rev.* **2020**, *246*, 106533. [[CrossRef](#)]
88. Jara, I.A.; Maldonado, A.; de Porras, M.E. Did modern precipitation drivers influence centennial trends in the highlands of the Atacama Desert during the most recent millennium? *Geo. Res. Lett.* **2022**, *49*, e2021GL095927. [[CrossRef](#)]

89. Kock, S.T.; Schitteck, K.; Mächtle, B.; Maldonado, A.; Vos, H.; Lupo, L.C.; Kulemeyer, J.J.; Wissel, H.; Schäbitz, F.; Lücke, A. Multi-centennial-scale variations of South American summer monsoon intensity in the southern central Andes (24–27° S) during the late Holocene. *Geo. Res. Lett.* **2020**, *47*, e2019GL084157. [[CrossRef](#)]
90. Lücke, A.; Kock, S.; Wissel, H.; Kulemeyer, J.J.; Lupo, L.C.; Schäbitz, F.; Schitteck, K. Hydroclimatic record from an Altiplano cushion peatland 24° S indicates large-scale reorganization of atmospheric circulation for the late Holocene. *PLoS ONE* **2020**, *17*, e0277027.
91. Torres, G.; Lupo, L.; Pérez, C. Reconstruction of the environmental conditions for the past 2,000 years in the Perico River basin (NW Argentina) based on fossil pollen records. *Veg. Hist. Archaeobot.* **2023**, *32*, 235–251. [[CrossRef](#)]

Disclaimer/Publisher’s Note: The statements, opinions and data contained in all publications are solely those of the individual author(s) and contributor(s) and not of MDPI and/or the editor(s). MDPI and/or the editor(s) disclaim responsibility for any injury to people or property resulting from any ideas, methods, instructions or products referred to in the content.